

Cite this: *Dalton Trans.*, 2020, **49**, 11902

Crystallinity after decarboxylation of a metal–carboxylate framework: indestructible porosity for catalysis†

Shengxian Cheng,^a Peter Tieu,^b Wenpei Gao,^c Jieying Hu,^{d,e} Weijin Feng,^a Jun He,^{id} *^d Xiaoqing Pan^{*c,f,g} and Zhengtao Xu^{id} *^a

We report a curious case study of a Zr(IV)-carboxylate framework, which retains significant crystalline order after cascade thermocyclization of its linker components, and – more notably – after the crucial carboxylate links were severed by heat. Vigorous heat treatment (e.g., 450 °C and above) benzannulates the multiple alkyne groups on the linker to generate linked nanographene blocks and to afford real stability. The resultant Zr oxide/nanographene hybrid solid is stable in saturated NaOH and concentrated H₃PO₄, allowing a convenient anchoring of H₃PO₄ into its porous matrix to enable size-selective heterogeneous acid catalysis. The Zr oxide components can also be removed by strong hydrofluoric acid to further enhance the surface area (up to 650 m² g⁻¹), without collapsing the nanographene scaffold. The crystallinity order and the extensive thermal transformations were characterized by X-ray diffraction, scanning transmission electron microscopy (STEM), IR, solid state NMR and other instrumental methods.

Received 11th June 2020,
Accepted 24th July 2020

DOI: 10.1039/d0dt02075c

rsc.li/dalton

Introduction

Post-synthetic annulation of organic linker molecules is a promising yet under-explored area in the study of metal–organic frameworks (MOFs) as a topical class of crystalline porous materials.^{1–7} As pioneered in a cross-cutting synthesis by the groups of Hupp, Farha and Stoddart,⁸ annulation of the spatially separated linker molecules in the rigid MOF scaffold allows their conversion into unique and discrete polycyclic aromatic hydrocarbons (PAHs) that cannot be accessed from the free-flowing solution medium, for the latter leads to stochastic

polymerization and the formation of amorphous precipitates. As PAH molecules often stack tight together to frustrate the assembly of open structures, such a two-step approach^{9–12} also serves to integrate PAHs and their highly polarizable π -electrons into the MOF matrix, in order to afford better photochemical and electronic properties. In a recent single-crystal-to-single-crystal transformation,¹³ the Zhou group applied Scholl oxidation/benzannulation to the elegant hexaphenylbenzene-based pbz-MOF-1 system¹⁴ and successfully achieved the large, fused PAH motif of hexabenzocoronene for enhanced photocatalytic reduction of CO₂.

Besides the intramolecular annulations, this group explored more complex cyclization processes that also covalently bridge the linker molecules in the MOF scaffold,¹⁵ in order to boost stability and charge transport, and to ultimately reach the field of porous carbon crystals (i.e., 3D graphene).^{16–18} The challenges, however, are obvious. Unlike the intramolecular reactions that preserve the well-defined connectivity of the coordination host, cyclizations involving intermolecular bond formation are highly dynamic, and often disruptive to the host lattice; and the amorphous products, besides being hard to characterize, would be deprived of the regular pore features vital for selectivity and reactivity control.

That is why our earlier tests on the alkyne-equipped linkers of H₂L1 and H₄L2 (Fig. 1a) had been instructive.^{15,19} In the Zr(IV)-based MOF solids formed therefrom, the contiguous alkyne units readily underwent thermocyclization (e.g., above 200 °C). While the tetratopic and more rigid L2-based ZrL2

^aDepartment of Chemistry, City University of Hong Kong, 83 Tat Chee Avenue, Kowloon, Hong Kong, China. E-mail: zhengtao@cityu.edu.hk

^bDepartment of Chemistry, University of California-Irvine, Irvine, CA, 92697, USA

^cDepartment of Materials Science and Engineering, University of California-Irvine, Irvine, CA, 92697, USA

^dSchool of Chemical Engineering and Light Industry, Guangdong University of Technology, Guangzhou, 510006, China

^eDepartment of Materials Science and Engineering, City University of Hong Kong, Kowloon Hong Kong, China

^fDepartment of Physics and Astronomy, University of California-Irvine, Irvine, CA, USA

^gIrvine Materials Research Institute, University of California-Irvine, Irvine, CA, USA

† Electronic supplementary information (ESI) available: General procedure, X-ray single-crystal structure of ZrL3, PXRD pattern for ZrL1, N₂ (77 K) sorption isotherms, CO₂ (195 K) sorption isotherms, solid-state ¹³C-NMR spectra, TGA spectra, EDX spectra, photographs of TLC plates, ¹H-NMR data of products from acetalization reaction and Pawley refinement results. See DOI: 10.1039/D0DT02075C

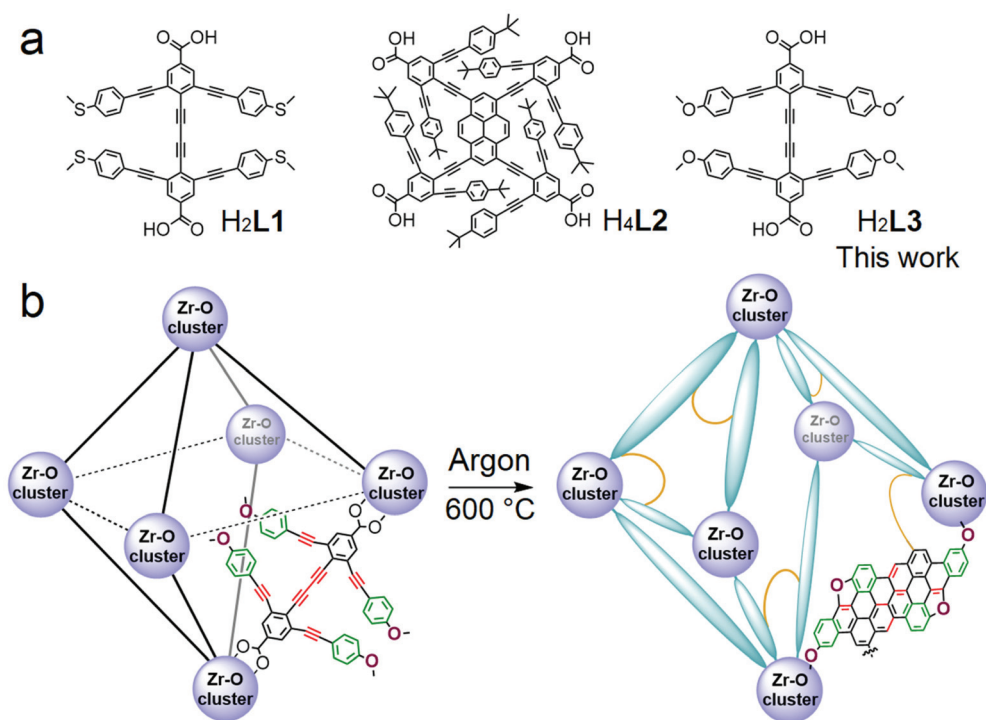


Fig. 1 (a) Three carboxylic linker molecules featuring backfolded side arms and conjugated alkyne groups; (b) scheme for the thermally induced linker benzannulation and decarboxylation of ZrL3 crystal (simplified as an octahedron-like unit). The resultant network contains linked nanographene blocks.

lost crystallinity upon thermocyclization, the linear and more supple L1-based ZrL1 afforded an ordered polycrystalline black covalent solid at up to 320 °C. Further covalent modification on ZrL1 (*e.g.*, cross-linking and ring fusion) at higher temperatures, however, resulted in an amorphous solid. It therefore remains desirable to develop MOF systems that can maintain crystallinity at higher temperatures, in order to further fuse the rings to emulate the fully conjugated 3D graphene—and to bridge the two fields of coordination and covalent solids.

Reported here is an advancement in this area: *i.e.*, the MOF crystal ZrL3 was found to remain ordered after undergoing extensive linker cyclization and significant fracturing at 400–600 °C (Fig. 1b). Surprisingly, the crystallinity of the host net persists even after the carboxylate strut of L3 was thermally ruptured, highlighting robust covalent bridges successfully established among the linker molecules. The resulting 3D graphene analog was stable in broad pH conditions from saturated NaOH to strong H₃PO₄ solutions, allowing size-selective, heterogeneous catalysis^{20–22} to proceed in its uniform pore systems.

Results and discussion

Crystallinity retention after being heated at 450 °C or above

The synthesis and characterization of molecule H₂L3 and the ZrL3 crystal (*P4/mnc*; $a = 24.758$ and $c = 31.932$ Å) were recently reported.²³ The X-ray structure of the ZrL3 framework,

Zr₆O₄(OH)₄(H₂O)₆(L3)₅(DEF)₂, merits a recap: its iconic Zr₆O₄(OH)₄ cluster²⁴ is linked to 8 L3 carboxyl groups in the regular, bidentate/straddling mode, and two in a monodentate mode, with other open sites taken by water or DEF molecules (Fig. S1†). Compared with the weakly diffracting and unsolvable sulfur analog ZrL1, the crystals of ZrL3 allow single crystal X-ray diffraction studies to locate the linker molecules of L3. The structural order of ZrL3 is perhaps enhanced by its more polar CH₃O[−] groups (*vs.* the thioether CH₃S[−] of ZrL1) that impose stronger intermolecular forces to order the molecules in the MOF matrix. In the dynamic, thermally induced cyclizing and splintering process, the chemically harder ether O atoms in ZrL3, swinging close to the Zr(IV) ion, offer a stronger binding with the latter, to help lock in the L3 components and the host lattice; as a result, ZrL3 exhibits a higher temperature (600 °C) at which crystallinity persists, relative to the temperature (320 °C) of ZrL1 (Fig. S2†).

The evolution of powder X-ray diffraction patterns as a function of temperature is revealing (Fig. 2). The as-made sample of ZrL3 displays a tetragonal cell ($a = 24.68$ Å, $c = 32.37$ Å; Fig. 2b; see Pawley refinement results in the ESI†) as is consistent with the X-ray single crystal structure. As for ZrL3-ac, *i.e.*, ZrL3 activated by exchanging with CH₃CN and then evacuating at 100 °C (formula: Zr₆O₄(OH)₆·(L3)₅(H₂O)₂), it exhibits broadened peaks that preclude unambiguous indexing, and the peaks are right-shifted to indicate unit cell contraction (Fig. 2c). The peak broadening (*e.g.*, due to partial framework collapse) and cell contraction can be ascribed to the dynamic

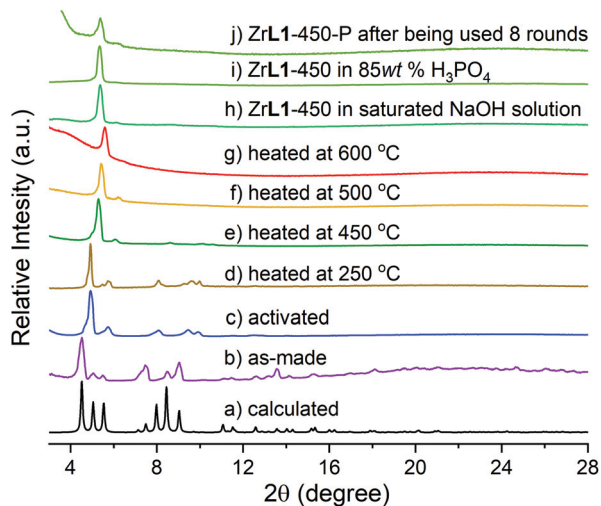


Fig. 2 X-ray powder patterns (Cu K α , $\lambda = 1.5418 \text{ \AA}$): (a) calculated from the single-crystal structure of ZrL3; (b) as-made ZrL3; (c) activated ZrL3 (ZrL3-ac); (d) ZrL3-ac heated at 250 °C for 2 h (ZrL3-250); (e) ZrL3-ac heated at 450 °C for 2 h (ZrL3-450); (f) ZrL3-ac heated at 500 °C for 2 h (ZrL3-500); (g) ZrL3-ac heated at 600 °C for 2 h (ZrL3-600); (h) ZrL3-450 soaked in a saturated water solution of NaOH overnight; (i) ZrL3-450 soaked in 85 wt% water solution of H₃PO₄ overnight; (j) ZrL3-450-P (ZrL3-450 soaked in the mixture of acetonitrile and 85 wt% H₃PO₄ aqueous solution with heating at 60 °C) after being used for 8 catalytic rounds.

bonding around the Zr–O cluster, as also documented elsewhere.^{25–27} Heating the activated sample ZrL3-ac at 250 °C for 2 hours affords the black powder of ZrL3-250, with IR and NMR (Fig. 4b and S3†) indicating full alkyne cyclization (but with retention of the carboxyl links).

ZrL3-250 gives a well-defined PXRD pattern (Fig. 2d) indexable onto a tetragonal cell ($a = 21.74 \text{ \AA}$, $c = 31.92 \text{ \AA}$; see the ESI† for the Pawley refinement). Heating ZrL3-ac at a higher temperature of 450 °C for 2 hours (to form the ZrL3-450 solid) induces decarboxylation and further linker fusion (IR and NMR, Fig. 4c and S3†), but retains significant crystalline order: the remaining PXRD peaks (Fig. 2e) suggest a tetragonal ($a = 28.92 \text{ \AA}$, $c = 29.07 \text{ \AA}$) or cubic symmetry ($a = 28.99 \text{ \AA}$, see the ESI† for the refinements) with the ambiguity due to limited diffraction data. Some crystalline order was maintained even after ZrL3-ac was heated at 500 °C for two hours, with two distinct peaks suggestive of a cubic lattice in ZrL3-500 ($a = 28.26 \text{ \AA}$; Fig. 2f). After treatment at 600 °C for 2 hours, the number of peaks further decreased, *i.e.*, with the only lowest-angle peak featuring in the powder pattern of the ZrL3-600 sample (Fig. 2g). Taken together, the gradual and continuous changes in the PXRD patterns, indicating no abrupt structural collapse over the broad temperature range, serve to highlight the resilience of the crystalline lattice originally imposed by the ZrL3 scaffold.

The ZrL3 samples treated at 450 °C and 600 °C were also examined by high angle annular dark field scanning transmission electron microscopy (HAADF-STEM). MOF systems are generally sensitive to the electron beam. By comparison, ZrL3-

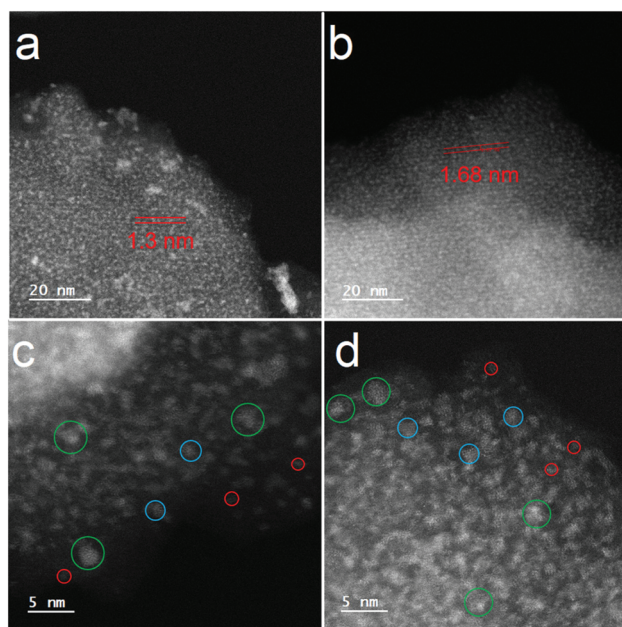


Fig. 3 HAADF-STEM images of (a) ZrL3-450 and (b) ZrL3-600 to show the lattice fringes of two samples with d -spacing; larger amplified images of (c) ZrL3-450 and (d) ZrL3-600 to exhibit individual clusters (around 0.8 nm; partially circled in red circles) and merged clusters at sizes of around 1.6 nm (partially circled in blue circles) and 2.0 nm (partially circled in green circles).

450 and ZrL3-600 did not exhibit additional evolution, such as further growth of the Zr–O clusters, during imaging. Spectroscopic analysis inside the microscope does induce aggregation of the Zr–O clusters, but the scanning time for spectroscopy is hundreds of times longer than that of imaging.

As shown in Fig. 3, the ZrL3-450 solids display ordered lattice fringes (arising from the ordered distribution of the heavy Zr–O clusters). The interplanar spacing shown is about 1.3 nm, which is comparable with that of the (0 0 2) plane (1.4 nm) calculated from the powder pattern e (Fig. 2). In accordance with the lower crystallinity observed by PXRD, the sample of ZrL3-600 displays fainter lattice fringes with a d -spacing of *ca.* 1.68 nm (Fig. 3b), which is close to the value determined from the main peak that featured in the PXRD (Fig. 2g). More notably, the STEM micrographs are dominated by the aggregated Zr–O clusters. As shown in Fig. 3c, cluster aggregation is found to be already extensive in the sample of ZrL3-450: *i.e.*, only a few individual, original Zr-clusters (around 0.8 nm) can be identified, while the majority feature larger sizes, around 1.6–2 nm, which result from several clusters being merged together. Similarly, ZrL3-600 exhibits clusters ranging from 0.8 nm to 2.0 nm, with the small, intact ones (0.8 nm) being even harder to spot.

Characterization of linker cyclization and decarboxylation

The extensive aggregation of the Zr–O clusters points to their large displacement and migration during the thermal treat-

ment, and such mobility may likely arise from the cleavage of the Zr-carboxylate links that had originally served to anchor the Zr-O clusters. As decarboxylation is a commonly occurring organic reaction, we wonder if this indeed happened in the samples of ZrL3-450 and ZrL3-600.

The decarboxylation and cyclization of the MOF scaffolds (*e.g.*, at 450 °C or higher) are evidenced in the various characterization studies. First, the IR spectra point to drastic changes in functionalities. Besides, the disappearance of the alkyne stretching at 2204 cm⁻¹ (*cf.* spectra a, b and c of Fig. 4) is consistent with the cascade cyclization of ZrL1 that was previously reported.¹⁵ Also, the sharp peaks at 1600 cm⁻¹ and 1398 cm⁻¹ in spectra a and b, arising from the asymmetric and symmetric stretching vibrations of carboxylate groups,^{28,29} are absent in spectra c and d. Instead, a new peak appears at around 1580 cm⁻¹, indicating the existence of aromatic C=C groups associated with graphitic skeleton.^{30,31} In addition, the C-H stretching from the CH₃O- groups (at 2836 cm⁻¹) is greatly diminished in ZrL3-450 and disappear in ZrL3-600, indicating the cleavage of the CH₃-O bond. With the departure of the methyl groups, the remaining oxygen atoms can annulate with the benzenoid carbons to form heterocycles, which might be responsible for the peak at 1259 cm⁻¹ (C-O-C asymmetric stretching) in spectrum c;³¹ or the O atoms can bond to the Zr(IV) centers as an aryloxide group (Fig. S3b†). As for ZrL3-600, the peak around 1259 cm⁻¹ disappears, which probably correlates with further loss of the oxygen atoms from the organic grid. The higher-temperature treatment (*e.g.*, at 600 °C) thus serves to further carbonize and aromatize the organic matrix, with its IR features having a closer resemblance to those of graphene or nanoribbons (Fig. S5†).^{32,33}

The ¹³C-NMR results also indicate decarboxylation and extensive cascade cyclization of the thermally treated samples. As seen in Fig. S3,† the carboxyl ¹³C peaks are absent in both the ZrL3-450 and ZrL3-600 samples, whereas in the sample ZrL3-250 and a reported carboxyl-containing sample (Fig. S6†),

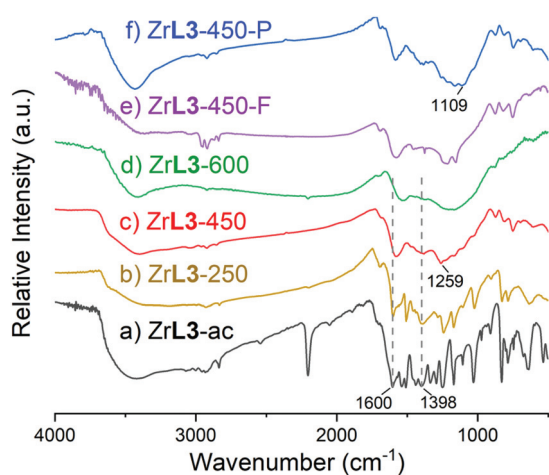


Fig. 4 FT-IR spectra for (a) ZrL3-ac; (b) ZrL3-250 (heated at 250 °C); (c) ZrL3-450; (d) ZrL3-600; (e) ZrL3-450-F (ZrL3-450 treated by HF solution); (f) ZrL3-450-P (ZrL3-450 treated by H₃PO₄ solution).

the ¹³C for carboxyl is distinctly featured at around 160 ppm. In addition, the peaks of alkyne, generally occurring between 70 and 90 ppm, disappear for both ZrL3-450 and ZrL3-600, as a result of thermal benzannulation. Instead, the ZrL3-450 solid displays two dominant signals at the aromatic area (the principal one at 128 ppm with a shoulder at 137 ppm), which can be largely rationalized by the proposed structure of Fig. S3.† Specifically, the latter signal (around 137 ppm) can be ascribed to the 14 edge quaternary carbons and 6 oxygen-bonded carbons, since these have been found to shift to a relatively low field in polycyclic aromatics;³⁴ the main peak at 128 ppm can be assigned to the remaining aromatic C atoms. By comparison, the shouldering feature (at 137 ppm) is largely suppressed in ZrL3-600, leaving a broad and more symmetrical peak centered at 128 ppm, which is consistent with more extensive carbonization throughout the solid state under higher temperatures, to render a structure more akin to graphene (see Fig. S3c;† as is also revealed in the evolution of the IR features observed above). Expectedly, the extension of the π -conjugated system significantly increases electrical conductivity from 10⁻⁵ S m⁻¹ for ZrL3-450 to 10⁻¹ S m⁻¹ for ZrL3-600 (preliminarily measured by a two-probe method), both of which also contrast the poor electrical conductivity (*i.e.*, below 10⁻¹² S m⁻¹) of the as-made and activated samples of ZrL3.

Thermal analysis (TG-DSC) indicates that the cyclization of linkers was triggered at around 250 °C with a significant release of heat without any obvious loss of weight (Fig. S7†). Around 0.7% of weight was lost at 100 °C due to the removal of 2 water molecules (coordinated guests). The onset decomposition occurred at about 385 °C followed by a rapid weight loss till 600 °C, which was most likely caused by the decarboxylation and demethoxylation of the linkers. To trace this decomposition process, stationary thermal treatments were then studied. The sample of ZrL3-ac was heated at fixed temperatures, *i.e.*, 450 °C and 600 °C, for 2 hours to afford black solid ZrL3-450 and ZrL3-600, respectively. ZrL3-450 displays a weight loss of 17% (Fig. S8†), which is attributed to dehydration (2 H₂O from the guest molecules and 3 H₂O from the cluster; totally 5 H₂O accounting for 1.9 wt%), decarboxylation (2 CO₂ per link; totally 10 CO₂ accounting for 9.2 wt%) and demethylation (4 CH₃ per link; totally 20 -CH₃ equivalent to 6.2 wt%). As for ZrL3-600, 7% additional weight loss occurred (relative to ZrL3-450, Fig. S9†), which may be caused by a partial shedding of the remaining O atoms (6.7 wt%, *e.g.*, in the form of CO); these O atoms are possibly fused with the aromatic grid or bonded to Zr(IV) in ZrL3-450 (Fig. S3b†).

Compared with the sulfur analog of ZrL1, such chemically hard O donors might better bond with the Zr(IV) centers, so as to help fix the Zr-O clusters in an ordered array at higher temperatures. The departure of these O anchors, *e.g.*, at 600 °C, unfortunately, led to a degradation of the structural order (with only one peak in the PXRD pattern and very faint lattice fringes in the STEM image, as mentioned above). It therefore remains a challenge to achieve a crystalline, ordered and carbonized organic grid from the MOF precursor. For future studies, the design of the linker shape and functional-

ity, as well as the choice of the MOF topology, should be closely coordinated, so that the thermocyclization of the linker pieces smoothly transit into a carbon crystal grid that carries over the crystalline order laid out by the MOF precursor.

Surface area, chemical stability, and cluster shedding

From a positive perspective, however, the degradation of crystallinity does not reduce the surface area—*i.e.*, the thermally treated samples remain highly porous. In particular, the CO₂ sorption isotherms at 195 K (Fig. 5 and Fig. S10†) indicate ever greater Langmuir surface areas from the as-activated (room temperature) sample to the 450 and 600 °C-treated samples: *i.e.*, 385 m² g⁻¹ for ZrL3-ac; 434 m² g⁻¹ for ZrL3-450; and 464 m² g⁻¹ for ZrL3-600. The thermocyclized solids therefore maintain the structural openness of the MOF precursor, and their increased surface areas are also consistent with the shedding of significant mass from the heated host grid. The N₂ uptake, by comparison, is not significant for all three samples (Fig. S11†), indicating the ultramicroporous (*e.g.*, pore size: <7.0 Å) nature of these materials. In general, the preferred sorption of CO₂ stems from its smaller kinetic diameter (330 pm), relative to N₂ (364 pm), its quadruple moment and the stronger thermal motion at 195 K (relative to 77 K for N₂).

The thermally treated samples exhibit extraordinary stability. For example, the ZrL3-450 solid retains the distinct PXRD profile (Fig. 2h) after being immersed in saturated NaOH solutions overnight. This compares favorably with the reported ZrL1-320 (ZrL1 heated at 320 °C for 3 hours under argon), whose crystallinity is largely destroyed even in a less concentrated 1 M solution of NaOH (Fig. S2†). Also, after being soaked in the highly corrosive H₃PO₄ (85 wt%, due to the high affinity of its dense O donors for the densely charged Zr⁴⁺ ions), ZrL3-450 remains crystalline (Fig. 2i); by comparison, phosphoric acid has proved especially detrimental to Zr(IV)-carboxylate networks.^{23,35}

The stability to strong bases and acids prompts the question: can one extricate the Zr(IV) oxide clusters to make for a

porous carbon framework? Indeed, heating a sample of ZrL3-450 in HF (48 wt%) at 80 °C for two days results in a solid product (ZrL3-450-F) depleted of Zr, as indicated by EDX analysis (Fig. S12†). Incidentally, the treatment by strong HF does not give rise to ν(COOH) peaks in the FT-IR spectrum of ZrL3-450-F (Fig. 4e; the feature around 1580 cm⁻¹ remains unchanged), further confirming the absence of carboxylate functions in the ZrL3-450 sample. The Zr-depleted structure ZrL3-450-F is non-crystalline as revealed by PXRD (Fig. S13†), but the specific surface area is greatly increased from 434 m² g⁻¹ (ZrL3-450) to 648 m² g⁻¹ (ZrL3-450-F, Fig. 5), indicating an amorphous yet highly porous aromatized framework. In general, 3D graphene-like carbon scaffolds attract great attention from theorists and synthetic chemists,^{17,36–38} with a popular preparative strategy being based on carbonization and/or chemical vapor deposition onto zeolites as templates.^{39–41} Unlike such drastic Aufbau from individual molecules, using ZrL3 and other cyclizable MOF solids as crystalline precursors offers more gradual and controllable passage onto the prospective carbon scaffolds. The diverse MOF topologies, together with the modifiable linker systems, not only allow various organic functions to be built into the carbon grid, but also offer hope for eventually achieving the coveted porous carbon crystals.

Heterogeneously catalyzed acetalization reaction

More imminent uses are also open for the robust thermocyclized solids. For example, ZrL3-450 readily anchors H₃PO₄ guests onto its Zr(IV) sites to make for a porous heterogeneous acid catalyst.^{42,43} Specifically, soaking the ZrL3-450 solid in a H₃PO₄ solution (1.0 mL of 85 wt% H₃PO₄ diluted with 2.0 mL of acetonitrile) affords the acidified sample ZrL3-450-P. The FT-IR spectrum (Fig. 4f) verified the loading of H₃PO₄ with a broad band around 1109 cm⁻¹ indicative of the stretching vibration of P–O–Zr. The P/Zr molar ratio was found to be about 1/4.5 by EDX analysis (Fig. S14†), corresponding to 1.3 H₃PO₄ molecules per Zr₆-cluster.

The solid acid ZrL3-450-P efficiently catalyzes the acetalization of both aldehydes and ketones, an important reaction widely used for masking carbonyl groups.^{44–46} The reaction can be done simply by heating the ZrL3-450-P catalyst and substrates (*e.g.*, P/substrate molar ratio: about 0.006/1) in toluene. Firstly, the benzaldehyde was chosen as the model substrate and ethanedithiol as the reagent. The reaction near-quantitatively was completed within 2 hours, while no product was detected when ZrL3-450 was used as the catalyst (indicated by TLC; Fig. S15†). The reaction most likely proceeded in a protonic acid catalyzed mechanism, with the substrate being activated for nucleophilic addition by protonating the carbonyl group with phosphorus acid anchored on the ZrL3-450-P scaffold. Acetophenone and other benzaldehyde derivatives substituted with either an electron-donating group or electron-withdrawing group were also smoothly converted into desired products with good yield, even though a prolonged reaction time was needed for 4-cyanobenzaldehyde (entry 4, Table 1). To illustrate that the catalyzation process was operating within

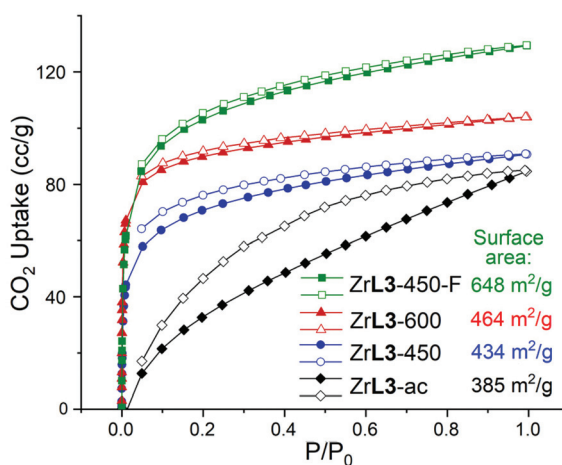


Fig. 5 CO₂ (195 K) adsorption and desorption isotherms for the samples of ZrL3-ac, ZrL3-450, ZrL3-600 and ZrL3-450-F.

Table 1 ZrL3-450-P catalyzed acetalization reaction between aldehydes/ketones and ethanedithiol/glycol

Entry	Substrates	<i>S,S</i> -acetal (yield) ^a	<i>O,O</i> -acetal (yield) ^a
1		 99%	 37% ^b
2		 91%	—
3		 96%	—
4		 88% ^c	—
5		—	Not tested
6 ^d		 97%	Not tested
7		—	 98% ^e
8		—	 98%
9		—	 99%

Reaction conditions: aldehydes or ketones (0.20 mmol), ethanedithiol or glycol (0.60 mmol), ZrL3-450-P (4.0 mg; the molar ratio of H₃PO₄ to substrates is 0.006/1), toluene (0.5 mL), 110 °C, 2 hours. ^a Determined by ¹H-NMR. ^b Reaction time was 20 hours. ^c Reaction time was 4 hours. ^d The 8th cycle. ^e Acetone was used as the solvent, reflux, 20 hours; “—” stands for no reaction.

the pores of the host net, a bulkier substrate, 3,5-bis(benzyloxy)-benzaldehyde (entry 5, Table 1), was used. No reaction proceeded even after 20 hours (as per TLC tests; Fig. S16†), in contrast to the smooth reaction homogeneously catalyzed by *p*-toluenesulfonic acid to form the expected dithioacetal product. Also, a test to examine the catalytic activity of the supernatant yielded a negative result (as shown by the NMR data in Fig. S17†), which indicates no leaching of the catalytic

species into the supernatant. Moreover, the recyclability of the crystalline ZrL3-450-P is highlighted in the constant yields observed in the 8 cycles tested: no obvious trend of catalytic activity loss was observed (entry 6, Table 1), and the crystallinity of the host framework persisted (as seen in the PXRD pattern (j), Fig. 2).

ZrL3-450-P also displays interesting chemoselectivity. For example, when aliphatic ketones were used as substrates, no corresponding *S,S*-acetals were obtained – with the starting materials unreacted (entries 6–8). However, when ethylene glycol was used, the selectivity reversed, with only aliphatic *O,O*-acetals obtained in high yield; while most of the aromatic ketones/aldehydes listed in Table 1 did not react (the benzaldehyde was sluggishly converted). This type of selectivity differed from reported cases, for example in cases where aldehydes were thioacetalized over ketones^{47,48} and aliphatic aldehydes were reacted preferentially over aromatic aldehydes.⁴⁹

Conclusions

Taken together, hybrid porous solids with extraordinary stability were achieved by using the cascade-cyclizing alkyne units of the linker molecules of metal–organic frameworks. A couple of key observations can be noted in this study. (1) The persistent porosity feature withstands not only the decarboxylation of the carboxylate linker, but also the extrication of the Zr-oxo blocks, highlighting the extensive bonding across the nanographene units generated from the thermocyclization process. (2) The crystallinity of ZrL3 can also survive the decarboxylation step (*e.g.*, at 450 °C), but appears to be quite sensitive to the order of the Zr–O components: for example, a higher temperature (*e.g.*, 600 °C) drastically moves and merges the Zr–O clusters, and diminishes the X-ray diffraction intensity as a result.

Looking ahead, opportunities for functionalization abound. For example, selective oxidization of the Zr-depleted nanographene grid should afford a porous 3D analog of graphene oxide. As the nanographene matrix is derived from the well-defined alkyne linkers of an ordered MOF scaffold, more uniform local features can be retained in the annulated solid, even in the absence of global crystallinity. Various O, S and halogen functions can therefore be affixed to the side arms, so as to be carried over into the thermocyclized framework.

One ultimate goal, however, lies in the appealing carbon crystals known as carbon schwarzites. For this, a carefully chosen MOF topology will have to work in close concert with the linker molecules of the fitting size and function. Besides the fundamental and practical importance of the carbon schwarzite, exploration towards this object will surely sharpen our skills in synergizing molecular design and solid-state synthesis.

Experimental

Crystallization and activation of ZrL3

The preparation and activation of the sample of ZrL3 was done according to the reported method.²³ Specifically, mole-

cule $\text{H}_2\text{L3}$ (20 mg, 0.025 mmol) and a *N,N*-diethylformamide (DEF, 0.75 mL) solution of ZrCl_4 (5.8 mg, 0.025 mmol) and acetic acid (300 mg, about 200 molar equivalents to ZrCl_4) were added in a Pyrex glass tube (soda lime, 10 mm OD, 6 mm ID). The tube was flame-sealed and heated at 120 °C in an oven for 48 hours, followed by programmed cooling to room temperature over 18 hours to afford orange truncated octahedron-shaped crystals (0.6–0.8 mm) with a yield of 35% based on $\text{H}_2\text{L3}$. For elemental analysis, the crystals were washed with DMF (3×1.5 mL) and soaked in acetonitrile (5×5 mL, replaced by fresh acetonitrile every 4 hours). The resulting crystals were then evacuated at 100 °C for 5 hours.

Preparation of the samples heated at various temperatures

The solid of ZrL3-ac was placed into a crucible, which was then transferred into a tube furnace. Afterward, the sample was heated to 250/450/500/600 °C at a rate of 5 °C min^{-1} under the protection of argon gas flow (40 mL min^{-1}) and maintained at this temperature for 2 hours, followed by cooling down to room temperature over 3 hours.

Preparation of the samples of ZrL3-450-P

The sample of ZrL3-450 (*e.g.*, 30 mg) was soaked in a mixture of H_3PO_4 (85 wt%; 1.0 mL) and CH_3CN (2.0 mL) and heated at 60 °C for 24 hours. Then the solid was isolated by centrifugation and thoroughly washed by heating in 2.0 mL of a mixture of CH_3CN and pure water (1:1, v/v) at 60 °C for 3 hours, with the solvent being replaced by a new batch every hour. Afterward, the sample was soaked in CH_3CN for 2–4 hours to remove the water molecules present inside the solids, followed by drying under dynamic vacuum at 100 °C for 7 hours.

Preparation of the sample of ZrL3-450-F

The sample of ZrL3-450 (50 mg) was heated in an HF aqueous solution (48 wt%; 3.0 mL) at 80 °C with stirring for 48 hours. Then the solid was isolated by centrifugation followed by heating in pure water (3.0 mL) at 60 °C for 3 h (replaced by fresh water every hour). Subsequently, the solid was solvent-exchanged with CH_3CN before being dried under dynamic vacuum at 100 °C for 7 h.

Preparation of the samples for HAADF-STEM image collection

The sample (ZrL3-450 or ZrL3-600) was ground with mortar and pestle to afford fine particles, which were then dispersed into 1 mL of ethanol in an Eppendorf tube. The resultant suspension was centrifuged at a relative centrifugal force of 3000 g for 5 minutes. The supernatant was collected and dispersed onto a holey carbon grid for HAADF-STEM measurement.

Typical conditions for heterogeneously catalytic reactions for the acetalization reaction

An aldehyde or ketone substrate (0.20 mmol), ethanedithiol or glycol (0.60 mmol), ZrL3-450-P (4.0 mg; the H_3PO_4 /substrate

molar ratio being 0.006:1), 1,2,4,5-tetramethylbenzene (internal standard) and toluene (0.5 mL) were loaded into a 3 mL glass vial. A gentle stream of N_2 gas outflowing from a Pasteur pipet was then placed slightly above the reaction mixture in the vial for about 30 seconds (this was for flushing the air in the vial); the pipet was then taken out, and the vial immediately capped. The reaction mixture was stirred by using a magnetic bar at 110 °C for several hours. After the reaction was completed (monitored *via* TLC), ZrL3-450-P was removed by centrifugation, and the supernatant was evaporated under reduced pressure, and the residue was examined by $^1\text{H-NMR}$ with the already added 1,2,4,5-tetramethylbenzene as the internal standard.

General procedure for recycling the catalyst ZrL3-450-P

After one round of the acetalization reaction between benzaldehyde and ethanedithiol, the catalyst of ZrL3-450-P was recovered by simple centrifugation and washed with toluene three times. After decanting the toluene, the solid was loaded into a vial together with a new batch of reactants and solvent for another catalytic cycle. The ZrL3-450-P heterogeneous catalyst was thus cycled 8 times, and no reduction in catalytic activity was found.

Catalytic activity test of the reaction supernatant

After running at 110 °C for one hour, a reaction mixture (using benzaldehyde and ethanedithiol; set up as above) was filtered for isolating the supernatant from the catalyst solid. Two drops of the filtrate/supernatant were added to CDCl_3 (0.5 mL) for ^1H NMR measurement. The rest of the supernatant was stirred at 110 °C for one additional hour, after which 2 drops were added to another 0.5 mL CDCl_3 for ^1H NMR measurement. The two NMR spectra thus obtained indicate the same ratio between benzaldehyde and 2-phenyl-1,3-dithiolane (the target product); in other words, no additional reaction was found in the supernatant after the isolation of the catalyst solid.

p-Toluenesulfonic acid catalyzed acetalization reaction between 3,5-bis(benzyloxy)-benzaldehyde and 1,2-ethanedithiol

The reaction was similarly set up as in the above heterogeneous catalysis, using 3,5-bis(benzyloxy)-benzaldehyde (31 mg, 0.10 mmol), 1,2-ethanedithiol (12 mg, 0.20 mmol) and *p*-toluenesulfonic acid (0.40 mg, dissolved in 0.4 mL of toluene). The reaction mixture was stirred at 110 °C for 18 hours (TLC indicating a strong new spot above the faint spot of the substrate) and then cooled back to room temperature and directly loaded onto a (microscale) pipet column (silica; eluted by 1:1 CHCl_3 /hexane, v/v). The yield thus obtained was 23 mg (58%).

Conflicts of interest

There are no conflicts to declare.

Acknowledgements

The work was supported by a GRF grant from the Research Grants Council of HKSAR (CityU 11306018), the National Natural Science Foundation of China (21871061), Local Innovative and Research Teams Project of Guangdong Pearl River Talents Program and Science and Technology Program of Guangzhou (2017BT01Z032).

Notes and references

- B. F. Hoskins and R. Robson, Infinite Polymeric Frameworks Consisting of Three Dimensionally Linked Rod-Like Segments, *J. Am. Chem. Soc.*, 1989, **111**, 5962–5964.
- G. B. Gardner, D. Venkataraman, J. S. Moore and S. Lee, Spontaneous Assembly of a Hinged Coordination Network, *Nature*, 1995, **374**, 792–795.
- S. Subramanian and M. J. Zaworotko, Porous Solids by Design: $[\text{Zn}(4,4\text{-bpy})_2(\text{SiF}_6)]_n \cdot x\text{DMF}$, a Single Framework Octahedral Coordination Polymer with Large Square Channels, *Angew. Chem., Int. Ed. Engl.*, 1995, **34**, 2127–21279.
- M. Kondo, T. Yoshitomi, K. Seki, H. Matsuzaka and S. Kitagawa, Three-Dimensional Framework with Channeling Cavities for Small Molecules: $\{[\text{M}_2(4,4\text{-bpy})_3(\text{NO}_3)_4] \cdot x\text{H}_2\text{O}\}_n$ (M = Co, Ni, Zn), *Angew. Chem., Int. Ed. Engl.*, 1997, **36**, 1725–1727.
- H. Li, M. Eddaoudi, M. O’Keeffe and O. M. Yaghi, Design and Synthesis of an Exceptionally Stable and Highly Porous Metal-Organic Framework, *Nature*, 1999, **402**, 276–279.
- A. Kirchon, L. Feng, H. F. Drake, E. A. Joseph and H. C. Zhou, From Fundamentals to Applications: A Toolbox for Robust and Multifunctional MOF Materials, *Chem. Soc. Rev.*, 2018, **47**, 8611–8638.
- J.-P. Zhang, Y.-B. Zhang, J.-B. Lin and X.-M. Chen, Metal Azolate Frameworks: From Crystal Engineering to Functional Materials, *Chem. Rev.*, 2012, **112**, 1001–1033.
- N. A. Vermeulen, O. Karagiari, A. A. Sarjeant, C. L. Stern, J. T. Hupp, O. K. Farha and J. F. Stoddart, Aromatizing Olefin Metathesis by Ligand Isolation inside a Metal-Organic Framework, *J. Am. Chem. Soc.*, 2013, **135**, 14916–14919.
- Y.-H. Kiang, G. B. Gardner, S. Lee, Z. Xu and E. B. Lobkovsky, Variable Pore Size, Variable Chemical Functionality, and an Example of Reactivity within Porous Phenylacetylene Silver Salts, *J. Am. Chem. Soc.*, 1999, **121**, 8204–8215.
- Z. Xu, S. Lee, Y.-H. Kiang, A. B. Mallik, N. Tsomaia and K. T. Mueller, A Cross-Linked Large Channel Organic Coordination Solid, *Adv. Mater.*, 2001, **13**, 637–641.
- T. Ishiwata, Y. Furukawa, K. Sugikawa, K. Kokado and K. Sada, Transformation of Metal-Organic Framework to Polymer Gel by Cross-Linking the Organic Ligands Preorganized in Metal-Organic Framework, *J. Am. Chem. Soc.*, 2013, **135**, 5427–5432.
- S. M. Cohen, The Postsynthetic Renaissance in Porous Solids, *J. Am. Chem. Soc.*, 2017, **139**, 2855–2863.
- J. S. Qin, S. Yuan, L. Zhang, B. Li, D. Y. Du, N. Huang, W. Guan, H. F. Drake, J. Pang, Y. Q. Lan, A. Alsalmeh and H. C. Zhou, Creating Well-Defined Hexabenzocoronene in Zirconium Metal-Organic Framework by Postsynthetic Annulation, *J. Am. Chem. Soc.*, 2019, **141**, 2054–2060.
- D. Alezi, I. Spanopoulos, C. Tsangarakis, A. Shkurenko, K. Adil, Y. Belmabkhout, M. O’Keeffe, M. Eddaoudi and P. N. Trikalitis, Reticular Chemistry at Its Best: Directed Assembly of Hexagonal Building Units into the Awaited Metal-Organic Framework with the Intricate Polybenzene Topology, pbz-MOF, *J. Am. Chem. Soc.*, 2016, **138**, 12767–12770.
- Y.-L. Hou, M.-Q. Li, S. Cheng, Y. Diao, F. Vilela, Y. He, J. He and Z. Xu, Dramatic Improvement of Stability by in Situ Linker Cyclization of a Metal-Organic Framework, *Chem. Commun.*, 2018, **54**, 9470–9473.
- H. Terrones and A. L. Mackay, Diamond from Graphite, *Nature*, 1991, **352**, 762.
- T. Lenosky, X. Gonze, M. Teter and V. Elser, Energetics of Negatively Curved Graphitic Carbon, *Nature*, 1992, **355**, 333–335.
- K. Kim, T. Lee, Y. Kwon, Y. Seo, J. Song, J. K. Park, H. Lee, J. Y. Park, H. Ihee, S. J. Cho and R. Ryoo, Lanthanum-Catalyzed Synthesis of Microporous 3d Graphene-Like Carbons in a Zeolite Template, *Nature*, 2016, **535**, 131–135.
- Y. Diao, J. Hu, S. Cheng, F. Ma, M. Q. Li, X. Hu, Y. Y. Li, J. He and Z. Xu, Dense Alkyne Arrays of a Zr(IV) Metal-Organic Framework Absorb $\text{Co}_2(\text{CO})_8$ for Functionalization, *Inorg. Chem.*, 2020, **59**, 5626–5631.
- L. Cao, Z. Lin, F. Peng, W. Wang, R. Huang, C. Wang, J. Yan, J. Liang, Z. Zhang, T. Zhang, L. Long, J. Sun and W. Lin, Self-Supporting Metal-Organic Layers as Single-Site Solid Catalysts, *Angew. Chem., Int. Ed.*, 2016, **55**, 4962–4966.
- Y. Sun, H. Huang, H. Vardhan, B. Aguila, C. Zhong, J. A. Perman, A. M. Al-Enizi, A. Nafady and S. Ma, Facile Approach to Graft Ionic Liquid into MOF for Improving the Efficiency of CO_2 Chemical Fixation, *ACS Appl. Mater. Interfaces*, 2018, **10**, 27124–27130.
- P. Ji, X. Feng, P. Oliveres, Z. Li, A. Murakami, C. Wang and W. Lin, Strongly Lewis Acidic Metal-Organic Frameworks for Continuous Flow Catalysis, *J. Am. Chem. Soc.*, 2019, **141**, 14878–14888.
- S. Cheng, K. Li, J. Hu, J. He, M. Zeller and Z. Xu, Building Conjugated Donor-Acceptor Cross-Links into Metal-Organic Frameworks for Photo- and Electroactivity, *ACS Appl. Mater. Interfaces*, 2020, **12**, 19201–19209.
- J. H. Cavka, S. Jakobsen, U. Olsbye, N. Guillou, C. Lamberti, S. Bordiga and K. P. Lillerud, A New Zirconium Inorganic Building Brick Forming Metal Organic Frameworks with Exceptional Stability, *J. Am. Chem. Soc.*, 2008, **130**, 13850–13851.
- S. Krause, V. Bon, U. Stoeck, I. Senkowska, D. M. Tobbens, D. Wallacher and S. Kaskel, A Stimuli-Responsive Zirconium Metal-Organic Framework Based on

- Supermolecular Design, *Angew. Chem., Int. Ed.*, 2017, **56**, 10676–10680.
- 26 J. S. Qin, S. Yuan, A. Alsalmeh and H. C. Zhou, Flexible Zirconium Mof as the Crystalline Sponge for Coordinative Alignment of Dicarboxylates, *ACS Appl. Mater. Interfaces*, 2017, **9**, 33408–33412.
- 27 Y. Zhang, X. Zhang, J. Lyu, K.-i. Otake, X. Wang, L. R. Redfern, C. D. Malliakas, Z. Li, T. Islamoglu, B. Wang and O. K. Farha, A Flexible Metal-Organic Framework with 4-Connected Zr₆ Nodes, *J. Am. Chem. Soc.*, 2018, **140**, 11179–11183.
- 28 L. Valenzano, B. Civalleri, S. Chavan, S. Bordiga, M. H. Nilsson, S. Jakobsen, K. P. Lillerud and C. Lamberti, Disclosing the Complex Structure of Uio-66 Metal Organic Framework: A Synergic Combination of Experiment and Theory, *Chem. Mater.*, 2011, **23**, 1700–1718.
- 29 J. Arenas and J. Marcos, Infrared and Raman Spectra of Phthalate, Isophthalate and Terephthalate Ions, *Spectrochim. Acta, Part A*, 1979, **35**, 355–363.
- 30 H. Guo, M. Peng, Z. Zhu and L. Sun, Preparation of Reduced Graphene Oxide by Infrared Irradiation Induced Photothermal Reduction, *Nanoscale*, 2013, **5**, 9040–9048.
- 31 M. Acik, G. Lee, C. Mattevi, M. Chhowalla, K. Cho and Y. J. Chabal, Unusual Infrared-Absorption Mechanism in Thermally Reduced Graphene Oxide, *Nat. Mater.*, 2010, **9**, 840–845.
- 32 M. Khandelwal and A. Kumar, One-Step Chemically Controlled Wet Synthesis of Graphene Nanoribbons from Graphene Oxide for High Performance Supercapacitor Applications, *J. Mater. Chem. A*, 2015, **3**, 22975–22988.
- 33 B. Ou, Z. Zhou, Q. Liu, B. Liao, S. Yi, Y. Ou, X. Zhang and D. Li, Covalent Functionalization of Graphene with Poly (Methyl Methacrylate) by Atom Transfer Radical Polymerization at Room Temperature, *Polym. Chem.*, 2012, **3**, 2768–2775.
- 34 T. Thonhauser, D. Ceresoli and N. Marzari, Nmr Shifts for Polycyclic Aromatic Hydrocarbons from First-Principles, *Int. J. Quantum Chem.*, 2009, **109**, 3336–3342.
- 35 C. W. Abney, K. M. L. Taylor-Pashow, S. R. Russell, Y. Chen, R. Samantaray, J. V. Lockard and W. Lin, Topotactic Transformations of Metal-Organic Frameworks to Highly Porous and Stable Inorganic Sorbents for Efficient Radionuclide Sequestration, *Chem. Mater.*, 2014, **26**, 5231–5243.
- 36 B. Liu, H. Shioyama, T. Akita and Q. Xu, Metal-Organic Framework as a Template for Porous Carbon Synthesis, *J. Am. Chem. Soc.*, 2008, **130**, 5390–5391.
- 37 H. L. Jiang, B. Liu, Y. Q. Lan, K. Kuratani, T. Akita, H. Shioyama, F. Zong and Q. Xu, From Metal-Organic Framework to Nanoporous Carbon: Toward a Very High Surface Area and Hydrogen Uptake, *J. Am. Chem. Soc.*, 2011, **133**, 11854–11857.
- 38 M. Tagami, Y. Liang, H. Naito, Y. Kawazoe and M. Kotani, Negatively Curved Cubic Carbon Crystals with Octahedral Symmetry, *Carbon*, 2014, **76**, 266–274.
- 39 A. A. Zakhidov, R. H. Baughman, Z. Iqbal, C. Cui, I. Khayrullin, S. O. Dantas, J. Marti and V. G. Ralchenko, Carbon Structures with Three-Dimensional Periodicity at Optical Wavelengths, *Science*, 1998, **282**, 897–901.
- 40 J. Rodriguez-Mirasol, T. Cordero, L. R. Radovic and J. Rodriguez, Structural and Textural Properties of Pyrolytic Carbon Formed within a Microporous Zeolite Template, *Chem. Mater.*, 1998, **10**, 550–558.
- 41 H. Nishihara and T. Kyotani, Zeolite-Templated Carbons - Three-Dimensional Microporous Graphene Frameworks, *Chem. Commun.*, 2018, **54**, 5648–5673.
- 42 J. Jiang, F. Gandara, Y.-B. Zhang, K. Na, O. M. Yaghi and W. G. Klemperer, Superacidity in Sulfated Metal-Organic Framework-808, *J. Am. Chem. Soc.*, 2014, **136**, 12844–12847.
- 43 G. Akiyama, R. Matsuda, H. Sato, M. Takata and S. Kitagawa, Cellulose Hydrolysis by a New Porous Coordination Polymer Decorated with Sulfonic Acid Functional Groups, *Adv. Mater.*, 2011, **23**, 3294–3297.
- 44 V. Geetha Saraswathy and S. Sankararaman, Chemoselective Protection of Aldehydes as Dithioacetals in Lithium Perchlorate-Diethyl Ether Medium. Evidence for the Formation of Oxocarbenium Ion Intermediate from Acetals, *J. Org. Chem.*, 1994, **59**, 4665–4670.
- 45 S. Naik, R. Gopinath, M. Goswami and B. K. Patel, Chemoselective Thioacetalisation and Transthoacetalisation of Carbonyl Compounds Catalysed by Tetrabutylammonium Tribromide (TBATB), *Org. Biomol. Chem.*, 2004, **2**, 1670–1677.
- 46 B. Procuranti and S. J. Connon, Unexpected Catalysis: Aprotic Pyridinium Ions as Active and Recyclable Brønsted Acid Catalysts in Protic Media, *Org. Lett.*, 2008, **10**, 4935–4938.
- 47 M. A. Ceschi, L. de Araujo Felix and C. Peppe, Indium Tribromide-Catalyzed Chemoselective Dithioacetalization of Aldehydes in Non-Aqueous and Aqueous Media, *Tetrahedron Lett.*, 2000, **41**, 9695–9699.
- 48 S. Muthusamy, S. A. Babu and C. Gunanathan, Indium Triflate: A Mild Lewis Acid Catalyst for Thioacetalization and Transthoacetalization, *Tetrahedron*, 2002, **58**, 7897–7901.
- 49 T. Sato, J. Otera and H. Nozaki, Differentiation between Carbonyls and Acetals in 1, 3-Dithiane and 1, 3-Dithiolane Synthesis Catalyzed by Organotin Triflates, *J. Org. Chem.*, 1993, **58**, 4971–4978.